Karlsruhe Institute of Technology

IEKP-KA/2013-8

# Your title
# in two rows
# or more

Master Thesis of


## Your Name

At the Department of Physics
Institut für experimentelle Teilchenphysik
(ETP)


| | |
|---|---|
| Reviewer: | Prof. Dr. Wim de Boer |
| Second reviewer: | Prof. Dr. Second Advisor |

Duration: 1. March 2017 – 28. February 2018

I declare that I have developed and written the enclosed thesis completely by myself, and have not used sources or means without declaration in the text.

**Karlsruhe, 18th January 2018**

. . . . . .

(**Your Name**)

# Contents

**Introduction** **1**

**1. Theory** **3**
1.1. Physic of cosmic rays . . . 3
1.1.1. Creation of CR . . . 3
1.1.2. Propagation of CR . . . 3
1.1.3. Gamma-ray creation . . . 4
1.1.4. Gamma ray observation . . . 5
1.2. What are the unresolved problems of the precedent chapter . . . 5

**2. Method** **7**
2.1. Data origin . . . 7
2.2. Model components . . . 9
2.2.1. Basic components . . . 9
2.2.2. Additional components . . . 11
2.3. Fitting method . . . 14
2.4. Introduction of results . . . 15

**3. Results** **17**
3.1. Recreating previous results . . . 17
3.2. Introducing SCR . . . 17
3.3. Introducing SCR and MCR . . . 18
3.3.1. Discussion on spatial shapes . . . 19
3.4. Introducing SCR and DM . . . 21
3.5. Introducing SCR and MSP . . . 21

**4. Discussion** **27**
4.1. Interpretation of spatial shapes . . . 27
4.2. Why is MCR better than DM or MSP . . . 27
4.3. How do these results fit in context . . . 27

**5. Conclusion** **29**

**Bibliography** **31**

**Appendix** **35**
A. Some appendix section . . . 35

# Introduction

Awesome introduction.

# 1. Theory

The theory chapter. These are references [1], [2], [3]. Figure **??** shows a placeholder.

## 1.1. Physic of cosmic rays

### 1.1.1. Creation of CR

### 1.1.2. Propagation of CR

Once they are emitted, the cosmic rays propagate through the galaxy under the influence of different interactions. The first one to notice is the complex manetic field created by all sorts of objects, from the stars to molecular clouds or any distribution of charged particles. It is not particularly strong **(put values)** compared to the heliosphere or what we can create on Earth, but its very large scale suffice to bend the CR's path in all direction until the point where it is impossible to backtrace its origin. An other possible interaction is the collisions with other particules. It will obviously depends on the density distribution of those colliders in the galaxy. We can expect a higher number of those in the disk, where the density of molecular clouds the highest. **ToDo**

All these influences can be modeled by a diffusion model, mainly defined by its diffusion coefficient, which discribes the average distance traveled in a certain time. The higher the coefficient, the faster a particule will diffuse in the galaxy. Each phenomenon can be attributed one of those coefficient to describe its effect on the cosmic rays. **(give values for Dmag, Dcoll...)** While the diffusion coefficient for the galactic magnetic field can be taken as constant throughout the milky way, the diffusion coefficient due to collision is proportional to the particles density. We can then expect a smaller coefficient in molecular clouds, where the density can reach **(value!)**. **ToDo** **ToDo**

This coefficient will also define the cosmic ray densities in various locations of the galaxy. Indeed, the more a particle's path is twisted and convoluted, the harder it will be to escape move away from its origin. This way, a higher density of cosmic rays can be found in low diffusion coefficient areas like molecular clouds. In comparison, the region outside the galactic disk has a low density of CR due to a weak magnetic field and small gas and dust density. However, the bubble region is outside the disk and has a

higher concentration of CR other regions outside the disk. This is due to a direct outward emission of CR from the GC region in the disk. With a high diffusion coefficient, those
ToDo CR are ejected light years away **(put values)**, forming two symetric region extending north and south up to 40 degrees in latitude.

### 1.1.3. Gamma-ray creation

Since the cosmic rays we observe on Earth can not give us a clue about their origin, some indirect detection methods are requiered. Luckily, cosmic rays interact n a lot of ways with their environment, as discribed in the previous section. These interactions can leave detectable traces that can be observed. The most common is the production of light, via creation of high energy photon in the GeV range. Once created, these gamma rays can be blocked or absorbed, but not deflected. Linking the gamma-ray and cosmic ray requires to know the processes in play. Her eis a list of the main phenomena.

#### 1.1.3.1. Pion decay

The high energy protons can produce $\pi^0$ which decay almost immediatly in 2 gammas of equal energy.

#### 1.1.3.2. Bremmstrahlung

The electrons passing near an other charged particle, or in a magnetic field will be deflected by the electromagnetic interaction. In the process, the electron will lose energy via the emmision of photons. The energy of the latter will depend on the energy of the electron and the intensit of the magnetic ield or the charge of the other particule. The
ToDo more the electron is deflected, the higher the energy of the emmitted photons. **(give numbers for B field and proton in MC)**

#### 1.1.3.3. Inverse Compton

A third interaction can link the cosmic ray electrons to gamma rays and it is inverse compton. When a high energy electron collides with a low energy photons, the electron can transfert some of its kinetic energy to the photon, giving him enough energy to enter the gamma range.

So number of gamma rays coming from inverse compton is directly linked tto the electron distribution and the interstellar radiation field (ISRF) of the galaxy. The latter is composed of three major components, the starlight, the dust emission and the cosmological microwave background (CMB). The first component is directly linked to the star distribution, and will be dominant in the disk, where all the star are concentrated. The starlight emits as a blackbody, peaking in the UV range. The dust emission comes from the infra-red emission of warm dust. It will also be mainly present in the disk, since the dust clouds are pretty flat. Finally, the CMB is peaking in the microwave range but is unformely present everywhere in the universe, and therefor in the galaxy. It will be dominant where the two others are negligeable, namely outside the galactic disk.

ToDo **(talk about synchrotron and ionization losses)**

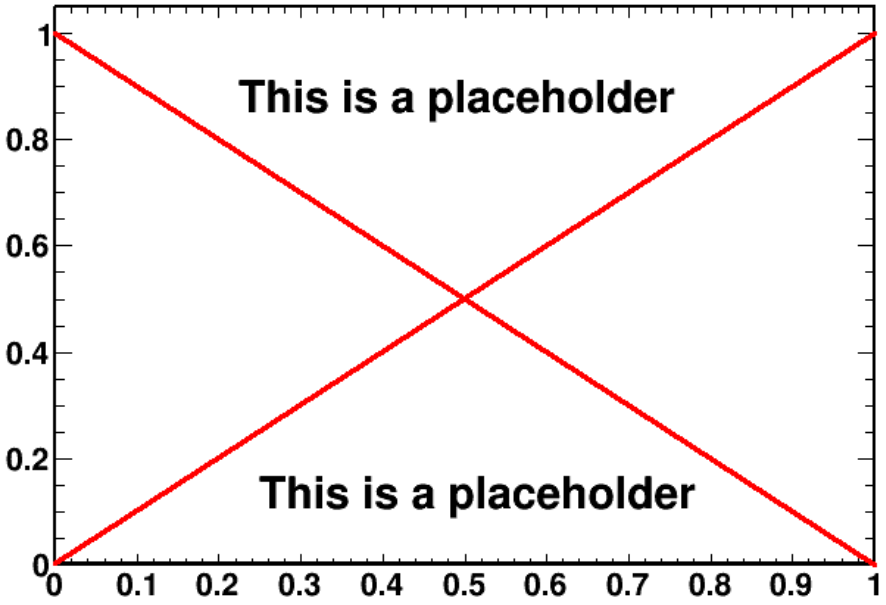


Figure 1.1.: chi2 distribution of first fits (not mines)

### 1.1.4. Gamma ray observation

Several instruments in the world observe gamma rays. For example the Fermi Large Area Telescope (LAT) mounted on the ISS. This instrument maps the gamma ray sky between 20MeV and 300GeV **(cite)**. The diffuse cosmic ray emmision that we are interested in can be obtained after modeling and subtracting the contribution of the over sources. This allows us to compare the observation with the models we obtain from the previous three interactions.

ToDo

## 1.2. What are the unresolved problems of the precedent chapter

Several studies have already tried to see how our predictions of the gamma rays emission and our observations compare. The three main phenomena were modeled as explained to try to recreate the spectrum observed from Earth. The results are clear, there are somethings missing in our interpretation. The fit is clearly not working in the galactic plane and the bubbles (as shown on Fig. 1.2. The spatial templates used in those fits also show a spherical excess of gamma rays of about 2GeV in the galactic center (GC).

Two main ideas have emerged to explain this spherical excess.

First is the presence of dark matter in the galaxy in the form of weakly interacting massive particles (WIMP). The spatial distribution of these particles would follow a Navarro-Frrank-White (NFW) profile centered at the GC. They are also expected to produce gamma rays when annihilating with each other via hadrons production. In theory, if the mass of a WIMP particle is around 50GeV, the expected gamma spectrum would peak around 2GeV, where the excess is observed. **(cite)** The study of the excess could put strong limits on the mass and annihilation cross section of such WIMP and confirm, or infirm the theory.

ToDo

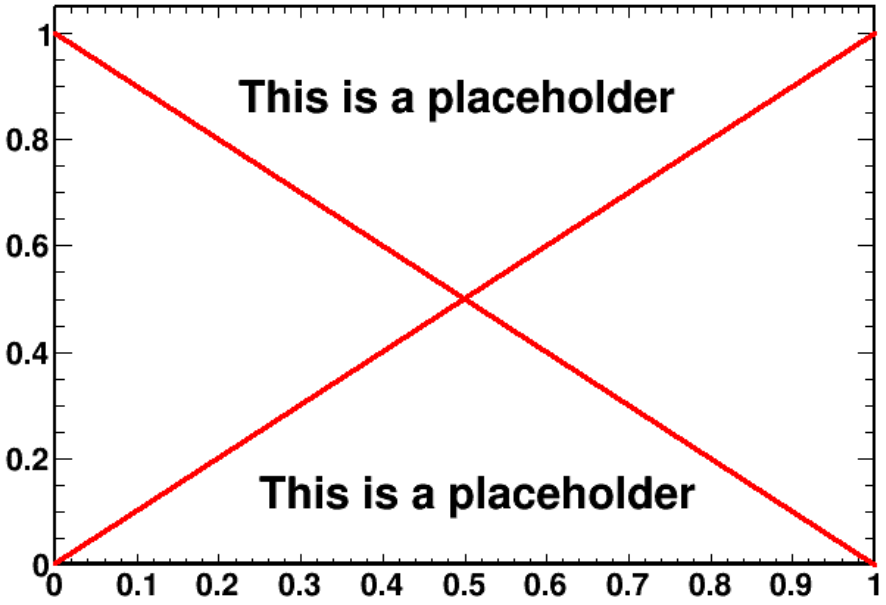


Figure 1.2.: shape of the excess

The second theory does not involve new physic, but inobserved milli-second pulsars. They would also be spherically distributed around the GC and their gamma spectrum peaks around 2GeV. A few thousands of them would be needed to recreate the intensity of excess. The main default of this explaination resides in the fact that we have observed only a few hundreds? at most. That would requires a very high concentration and a reason why we can not observe them more easely.

# 2. Method

The following chapter will present the the general method and the tools used through the internship.

## 2.1. Data origin

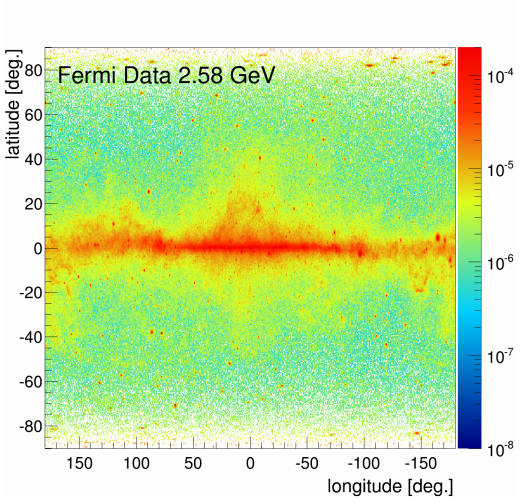


(a) Raw data flux from the LAT

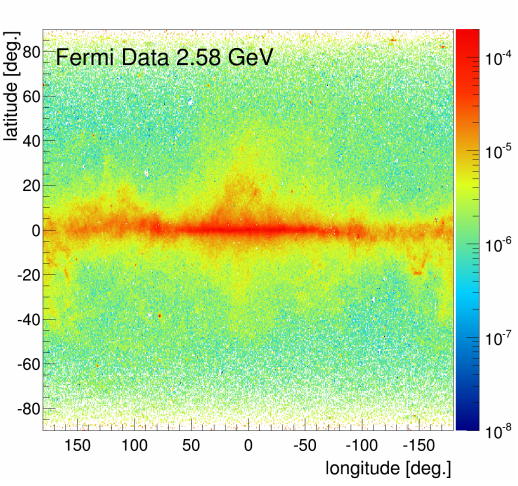


(b) Raw data with point sources fromn 3FGL catalog subtracted.

Figure 2.1.: Figures of data before and after point source subtraction. (Maybe also some spectrum with pass7 and pass8 to see the differences.)

First of all, all the following work is based on the measurement of gamma rays coming from the milky way and beyond. The quality and accuracy of the data points is one of the most important point that will determine the general quality of the results. Thus it is capital to be sure that the gathering and treatment of the data was done properly.

The data used in the next chapters was observed by the Fermi collaboration Large Area Telescope (LAT) between 2008 and today. They are available on the web and can be

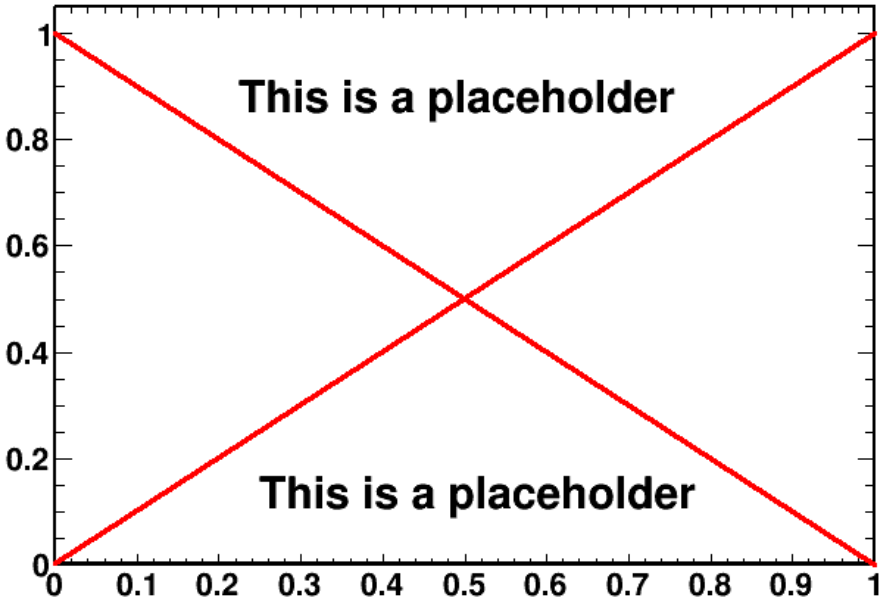


Figure 2.2.: Images of the exposure map

treated by anybody using the software given by Fermi.

Since the observation is still on-going, it is important to stay up-to-date. The treatment method of the data is also being improved regularly, resulting, among others, in better statistics, better systematic errors, wider energy range and better point source subtraction. One of the most important step in the treatment process is the first one, the selection of events. Every photon measured is saved along with all its properties in a big data file. Then this long list has to be filtered to keep only the interesting observations. The filter can be based on the incoming direction, the energy or the time of observation, but also on the quality of the event reconstruction. This last cut can be critical. It will determine if the chances that the measured event is in fact a gamma ray, and not some background noise polluting the data. Of course, the more strict is the filter, the less events are kept for analysis and the statistical errors can become large. This work uses the CLEAN class recommended by the Fermi team for diffuse analysis.

The details of the selection can be found in Tab 2.1.

An other important point is the creation of the exposure map of the telescope. It is basically a map of the time the telescope spend observing a portion of the sky. It is used to correct for an observation bias. If the telescope observed the galactic center ten times more often than the Orion nebula for example, there is no way to know at first if the higher counts in the GC are due to the longer exposition time or a higher incoming intensity. After dividing the count map by the exposure map, a flux map is obtained that does not depends on the observation time of particular regions.

The goal of this work is to study the diffuse sources of gamma-rays from inside and outside the milky way. Of course, the LAT does not differentiate between gamma rays coming from a pulsar or a cosmic ray. This has to be done manually as the last step of the treatment process. A large catalogue of gamma ray point sources (3FGL) is available

| Parameter name | Parameter value | Description |
|---|---|---|
| Event class (evclass) | 256 | Quality parameter. Varies the level of background noise. |
| Event type | 3 | Back+front event. |
| tmin, tmax | INDEF | Selecting all events since beginning of observation |
| Emin (MeV) | 58.4731 | Minimum energy of the event. |
| Emax (MeV) | 513056 | Maximum energy of the event. |
| zmax (degrees) | 90 | Maximum zenith angle to get rid of the Earth limb contaminations, as recommended by the LAT instrument team |

Table 2.1.: Parameter values for Fermi data selection

online on NASA website. This catalogue lists most of the known and identified point sources, along with their spectral shape and flux. These informations can be then used, combined with the exposure map, to model the number of counts coming from point sources, their spatial and energy distribution. Once this model map is done, it is subtracted from the data to keep only the diffuse emission. Of course the models are never perfect and all point sources are not listed. This can lead to errors or anomalies in the observations and this is an other reason to keep the dataset up-to-date.

Once all of the treatment is done, a flux map of the entire sky in $counts/s/m^2/GeV/sr$ is produced. The map is divided in bins of $0.5 \times 0.5$ degrees on a Cartesian projection. Every bin contains 30 logarithmic energy bins ranging from 60 MeV to 513 GeV with 1.2 multiplicative step. The final data cube is therefore of dimension $720 \times 360 \times 30$.

For visibility purposes, every energy bin is multiplied by its energy squared, becoming an energy flux in $GeV/s/m^2/sr$.

The errors on the data are come from two sources. The first are systematic errors due to the instrument or the treatment process. They are pretty low, around 3%, but can change for low or high energies as seen in Fig. 2.3. The other source is the statistical errors, simply proportional to the square root of counts (N). The final equation is given as follow :

$$\sigma_{tot} = \sqrt{\sigma_{sys}^2 + \sigma_{stat}^2} = \sqrt{\sigma_{sys}^2 + \frac{1}{N}} \tag{2.1}$$

## 2.2. Model components

### 2.2.1. Basic components

#### 2.2.1.1. $\pi^0$ production by propagated cosmic rays (PCR)

The initial propagated proton spectrum for the PCR template is obtained from the locally observed proton data from AMS-02 **(cite[55])**. A good approximation is an unbroken power law $(R-\alpha)$ with a spectral index $(\alpha)$ of 2.85 at rigidities above 45 GV. At lower rigidities the data are below the power law because of solar modulation **(cite[56])**, as can be seen from Fig. 2.4a, where the AMS-02 data are plotted as well. To find the best

**ToDo** **ToDo**

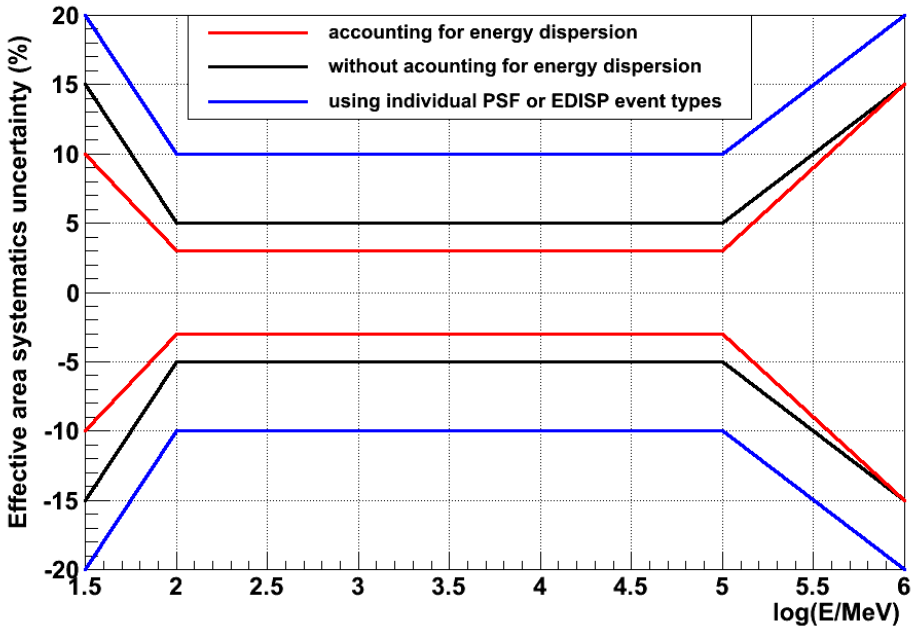


Figure 2.3.: Systematic error for Pass 8 data.

parametrization a set of broken power laws with a grid of breaks and spectral indices above and below the break was constructed and the optimal parametrization was found by interpolation between the fits with the best test statistic. The gamma-ray data are well described by an unbroken power law for the protons with a spectral index ($\alpha$) of 2.85 at all rigidities.

There is also the possibility to introduce a break around a few GeV, to have a slightly harder spectrum at lower energies.

#### 2.2.1.2. Inverse compton (IC) and bremmstrahlung (BR)

ToDo The interstellar electron spectra needed a break around **(1 GeV)** with a spectral index of 3.21 above the break, which is compatible with the locally observed electron spectrum (see Fig. 2.4b). Below the break the optimal spectral index is 0.81, which implies a suppression of electrons. The break point might be related to the fact that around 1 GeV electrons have the smallest energy losses, since above this energy synchrotron, BR and IC dominate the energy losses, while below this energy ionization losses become strong, thus depleting the electron spectrum below 1 GeV. A similar break in the electron spectrum was needed in the Fermi diffuse model **(cite[46])**.

ToDo

The targets for the production of gamma-rays are the interstellar gas and the interstellar radiation field, which are both stronngly dependant of position, , so the photon composition varies with sky direction. Hence, for the IC templates we have to calculate the templates for each sky direction. The variation over the sky is about ±10%, as shown in ??; for the BR template the spread is considerably smaller, as shown in ??.

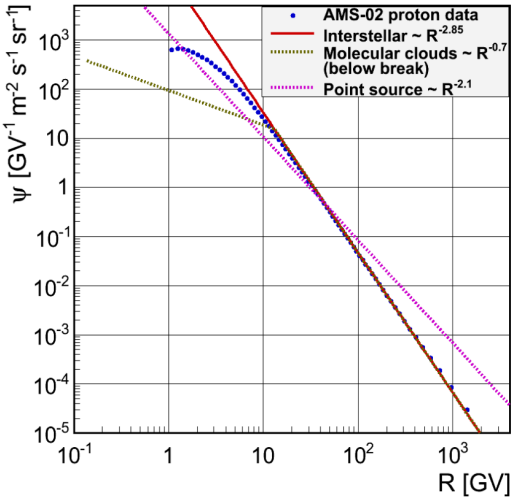


(a) images for proton spectrum for PCR, MCR, SCR, data

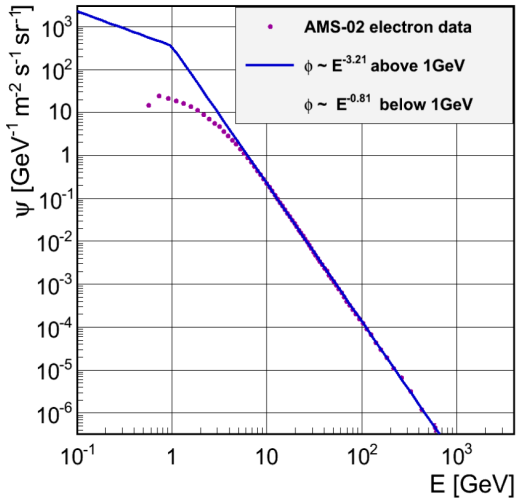


(b) images for electron spectrum for IC, BR, data

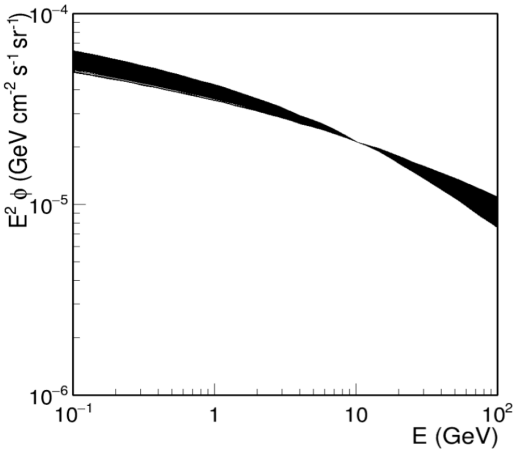


(a) images IC and BR variations over the sky

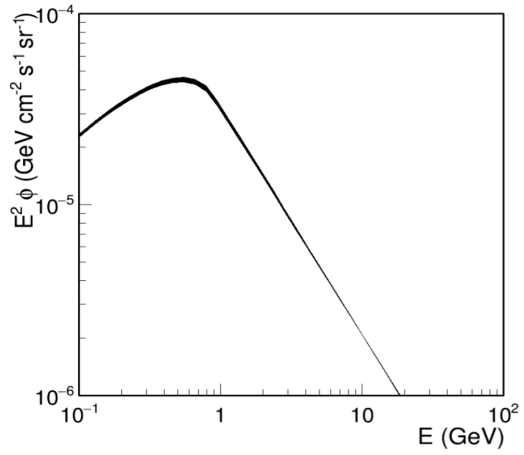


(b) images IC and BR variations over the sky

Figure 2.5.

## 2.2.2. Additional components

### 2.2.2.1. SCR component

The proton spectra for the SCR template can be described by an unbroken power law with a spectral index of 2.1, as obtained from the best fit. The index 2.1 for the SCR template agrees with the data from the Fermi Bubbles, shown by the data points inside the shaded band in Fig. 2.4a; the index 2.1 is expected from diffuse shock wave acceleration. **(cite[60, 61])** The fact that the Fermi Bubbles and the cosmic rays inside sources have the same spectrum strongly suggests that they are connected by point sources providing advective outflows of gas in the Galactic center. **(cite[44])** **ToDo** **ToDo**

### 2.2.2.2. MCR component

The decreasing gamma-ray emissivity from MCs below 2 GeV could be parametrized by a break in the power law of the corresponding proton spectrum. Above the break the optimal spectral index of 2.85 was found to be the same as for the PCR spectrum, as

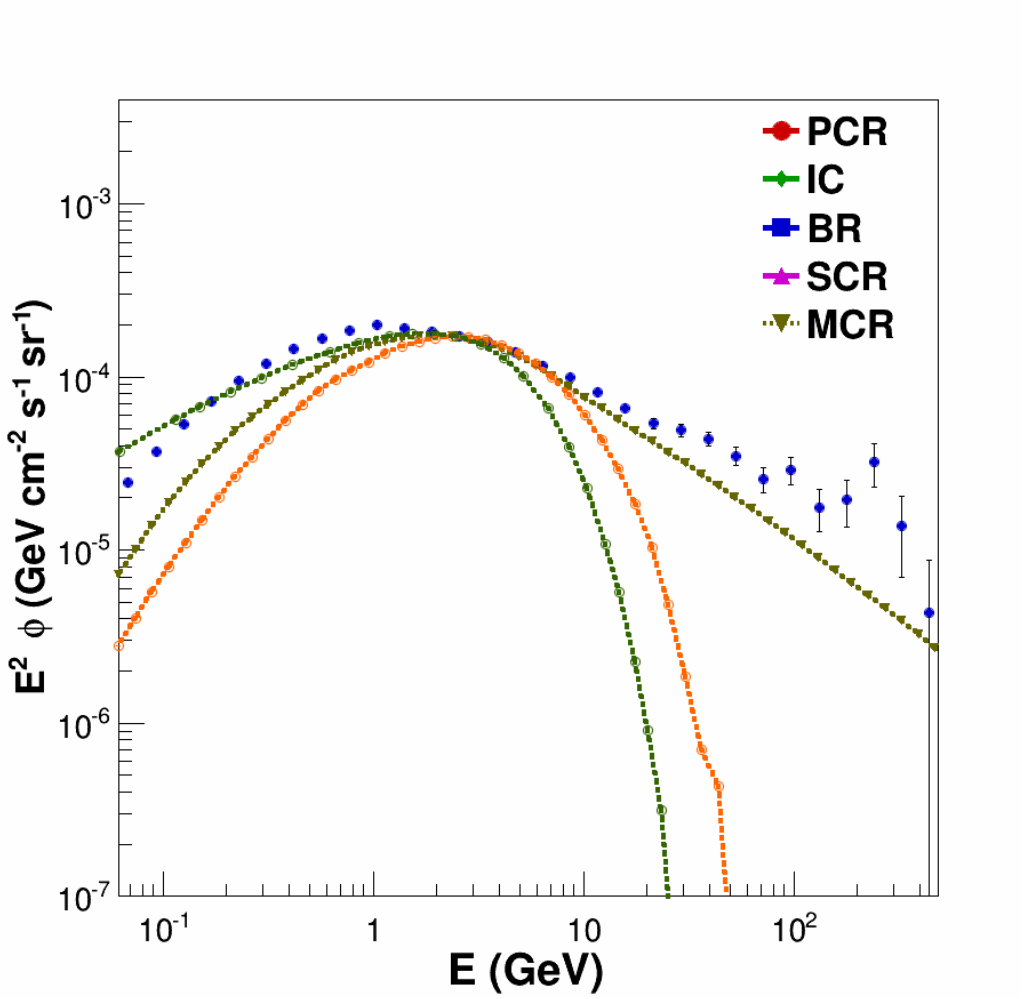


Figure 2.6.: images of MCR, MSP, DM on single plot.

expected if the high energy propagated protons are above a certain magnetic cutoff. But below the break, which varies according to the fit from 6 to 14 GV for the different clouds, the optimal spectral index is 0.7, thus providing a significant suppression of protons below the break, as can be seen from Fig. 2.4b. Energy losses alone cannot reproduce such a suppression of the proton spectrum below the break, but magnetic cutoffs are able to do so. Such a cutoff is well known from cosmic rays entering the Earth's magnetic field: particles below typically 20 GV entering near the magnetic equator do not reach the Earth, but are repelled into outer space by the geomagnetic cutoff. **(cite[62])** The **ToDo**
rigidity cutoff of 20 GV is proportional to the magnetic moment. Although the magnetic field near the Earth (0.5 G) is orders of magnitude higher than the typical magnetic fields in dense MCs **(cite[63])**, the much larger sizes of MCs - or its substructure of filaments **ToDo**
and cloudlets **(cite[64])** - yield magnetic moments of the same order of magnitude as **ToDo**
the Earth's magnetic moment, so similar magnetic cutoffs are plausible. Variations in the magnetic cutoff in MCs are expected from the variations in size and in magnetic field; the latter increases with MC density. **(cite[63])** The variations of the break in the **ToDo**
proton spectrum between 6 and 14 GV varies the maximum of the gamma-ray spectrum from 2 to 1 GeV**(??, as shown in Fig. ref??)**. The fit prefers a constant spectral index **ToDo**
below the break for all sky directions. Such a constant spectral index is plausible with regular magnetic fields oriented in the disk **(cite[65, 66])** and the "cloudlets" inside MCs **ToDo**
**(cite[64])** form magnetic dipole fields. Then the maximum cutoff occurs for cosmic rays **ToDo**
entering from the halo perpendicular into the cloud for any orientation of the magnetic dipole. For a given entrance angle the cutoff would provide a sharp break, but for an isotropic distribution of entrance angles the break points are smeared. A distribution of break points will provide a slope below the maximum break determined largely by the isotropic distribution of the entrance angles into the disk. Since this distribution is the same for all MCs the slopes below the break will be similar for all MCs, even if the maximum break (= maximum magnetic cutoff) varies.

#### 2.2.2.3. Dark matter (DM)

DM particles are expected to annihilate and just like in electron-positron annihilation the annihilation energy of roughly twice the WIMP mass will lead to the production of hadrons, thus producing copiously gamma-rays from $\pi^0$ decays. A smaller fraction of WIMP annihilation is expected to lead to tau lepton pairs, which can lead to $\pi^0$ production in the hadronic tau decays. This contribution is expected to be small and is neglected. The DM template can be calculated with DarkSusy. **(cite[67, 68])** The an- **ToDo**
nihilation signal peaking at 2-3 GeV requires a WIMP mass around 45 GeV, as shown in Fig. 2.6 as well. The difference to the MCR template is the cutoff at twice the WIMP mass, which is absent in the MCR template.

#### 2.2.2.4. Milli-second pulsars (MSP)

The MSP spectrum is directly taken from the Fermi study **(cite Fermi)** **ToDo**

#### 2.2.2.5. Isitropic component

The isotropic template represents the contribution from the isotropic extragalactic background and hadron misiden-tification. Its spectral shape and absolute normalization are provided within the Fermi software. **(cite[51])** The isotropic template was redetermined **ToDo**
for our analysis in the following way.

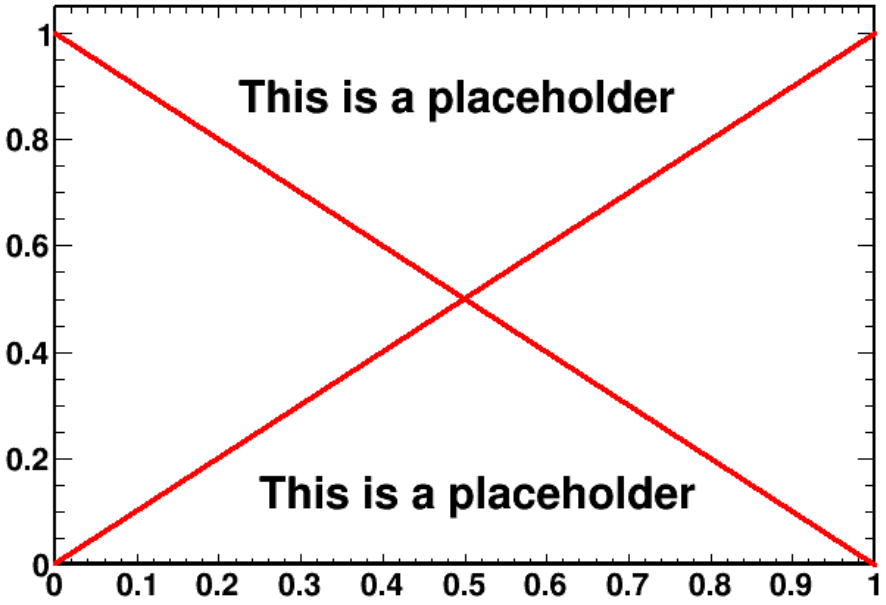


Figure 2.7.: Images to illustrate isotropic calibration

We fit the data in regions outside the Bubbles and Galactic disk using the isotropic template from the Fermi software as an initial estimate in the fit. If one plots the total observed gamma-ray flux versus the fitted flux in the various cones in a certain energy bin, one expects a linear relation crossing the origin, if the isotropic flux is estimated correctly. However, if there is a missing or too high isotropic contribution, this leads to an offset at the origin of the linear curve, since the isotropic component is by definition the same for all cones, so it shifts the whole curve up and down for each energy bin. An example of such a fit is shown in Figure 2.7 for an energy bin between **(3.7-5.2 GeV)**. The offset can be determined for each energy bin, which yields the spectral template of the isotropic component. The final spectral template is obtained by iteration until zero offset at the origin is reached. The resulting template in our analysis has deviations from the Fermi template up to 35% above 2 GeV, as shown in the insert of 2.7.

ToDo

## 2.3. Fitting method

The fitted data can be seen as a data cube whose dimension are longitude, latitude and energy. The finest spatial grid is divided in $720 \times 360$ cones of $0.5° \times 0.5°$. Every cone contains 30 energy bins. This allows to treat different portions of the sky independently of one another. Since the cones do not have the same solid angle and the statistic in a small bining can be problematic, the grid used is more often composed of 797 cones of different sizes, bigger at the poles or and smaller near the equator. This allows a better statistic in lower flux regions at high latitudes and where the resolution is less important. In the same time, the equator and the GC have a lot more counts and can be treated in a smaller binning. It is also way faster to compute.

The fits are done in the following way for every bin independantly. After choosing the templates used for the fit, their scaling factor is only degree of freedom allowed. Using a

ROOT TVirtualFitter object, every template is scaled up or down until their sum comes the closest to the data. Mathematically, the minimum distance between the model and the data is found when the $\chi^2$ value is lowest. It is calculated as follows:

$$\chi^2 = \sum_{i=1}^{30} [\frac{(D_i - \sum_{j=1}^{n} n_j.T_{ij})^2}{\sigma^2}] \tag{2.2}$$

where:

- $D_i$ is the data flux in the $i^th$ energy bin.
- $n_j$ is the scaling factor for the $j^th$ model component.
- $T_{ij}$ is the model flux of the $j^th$ in the $i^th$ energy bin.
- $\sigma_i$ is the geometric mean of the statistical and systematical error of the Fermi data point $i$.

The fit is very well constrained with only five or six degrees of freedoms depending on the fit against 30 data points. A usefull value is the $\chi^2/d.o.f$ where $d.o.f = \#data\,points - \#degrees\,of\,freedom - 1$. This rescaling has the advantage to bring the perfect $\chi^2$ value down to one, thus making the comparison between different fits easier. This rescaling will be applied everytime when speaking about $\chi^2$ in the rest of the discussion, except if explicitly told. The closest a $\chi^2$ value is to one, the better the model follows the data. The higher it gets, the lower the quality of the fit. It can also happen that it gets lower than one. This can happen when the fit is good, but the error bars on the data are too big.

Since every bin is fitted independantly, it is not possible to implement a spatial template, i.e. where the spatial shape of a component would be fixed in advance. For example a component with a spherical distribution around the GC, as can be done in other works **(cite)**. The hope is to let the fit find reasonnable shapes by itself only using the $\chi^2$ minimization technique. **ToDo**

## 2.4. Introduction of results

This fitting method offers multiple ways of looking at the results depending on what is the interest. It is possible to produce flux skymaps of each component to study their spatial shapes, or spectrum of one particular region to look at the relative quantity of every template at different energies.

The first step when testing a new model, is to see if it can reproduce results of previous studies. Only once it works and can be confidently used can it be

Recretion of previous studies (GC excess, problems).
Introduction of new component to take care of those problems (SCR for high energies, MCR, Dm or MSP for 2GeV excess)

# 3. Results

## 3.1. Recreating previous results

Introduce the weniger plots here (or in the state of the research?) to show excess in GC.

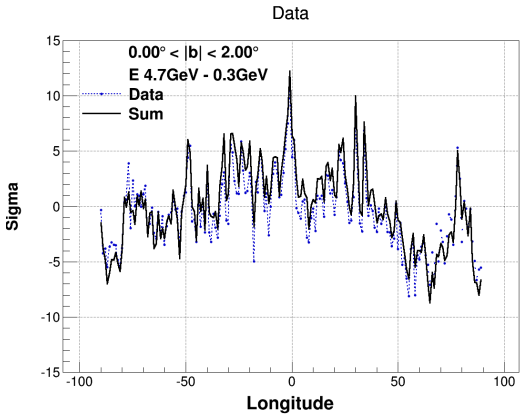


Figure 3.1.: Some weniger plots to show the GC excess

Before trying upgrade the model in use, it is important to make sure we can recreate it with the same parameters. Fig. 3.2 shows the results of a fit using only the PCR, IC and BR components. The shape and intensity of the previously observed excess are found **(cite)**. **ToDo**

It can also be observed that the fit is particularly bad in the bubbles and the disk (see Fig. 3.2) where the high energy spectrum is harder (see Fig. 3.3). In this region, the PCR spectrum falls off too quickly, and the IC spectrum which usually takes care of high energies is blocked by the low energy flux drop.

## 3.2. Introducing SCR

Introducing the SCR template, a clear improvement can be noted in the $\chi^2$ distribution (see Fig. 3.4). The bubble shape that was clear before has now disapeared. Even if the fit is still not perfect everywhere, the improvement is significant.

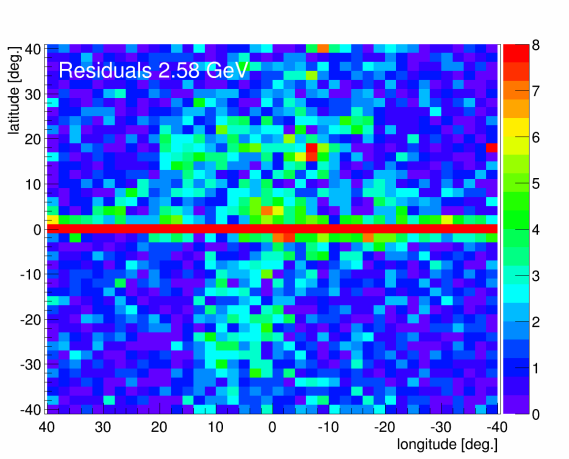


Figure 3.2.: Picture of GC excess, (compare with previous papers?), a chi2 map too

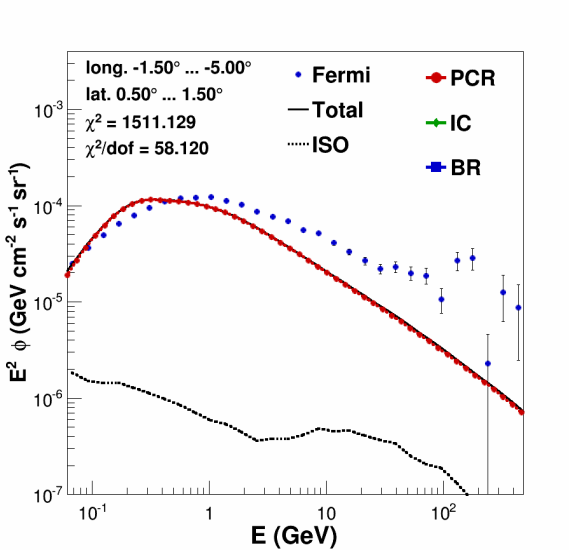


Figure 3.3.: Picture background only spectra with bad fit (high energies too hard) Compare bubble or disk region and outside

From Fig. 3.5a and 3.5a we see the role of the SCR template at high energies, taking care of the high flux. It also permits a better fit of low energies by PCR and IC since they do not have to be everywhere at the same time.

ToDo **(Here the bad chi2 comes from 0.1GeV region, where the PCR template does not fit the data. not from the 2GeV excess.)** A problem still remains in the disk and diffuse regions around the galactic anticenter.

## 3.3. Introducing SCR and MCR

As shown on Fig. 3.6, the addition of a new template improve significantly the $\chi^2$ distribution in all directions. The bubbles and the disk structures are not visible anymore.

Three dots appear to have a really high $\chi^2$, but that is only due to the point source subtraction that is not perfect (see Chapt. 2.1).

Fig. **??** shows the central molecular zone (CMZ) fitted with and without the MCR component. The gas density is very high in this region, hence it is the first region where we

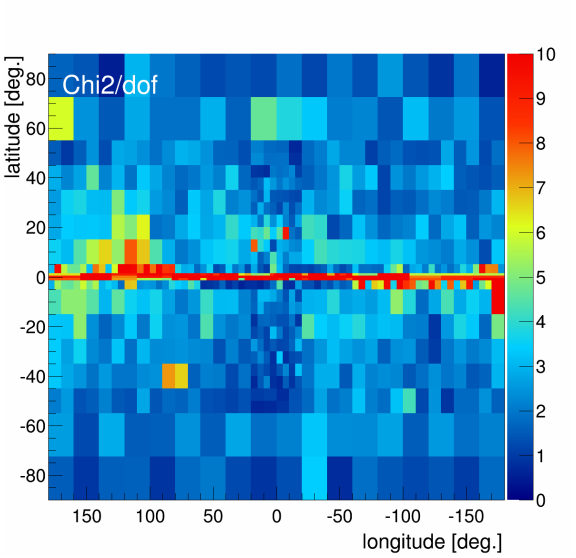


Figure 3.4.: Chi2 distribution of SCR only fits.

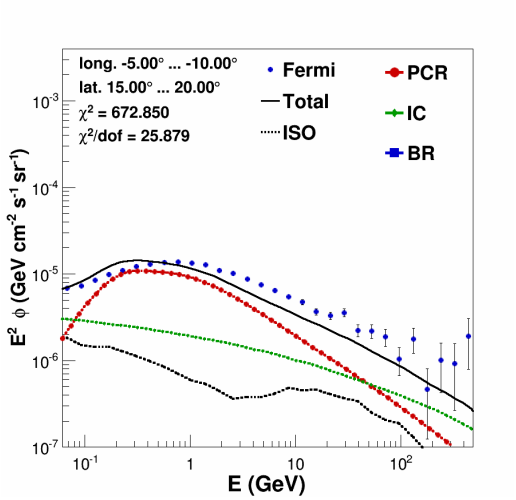


(a) Spectrum from a bubble with SCR only and background only.

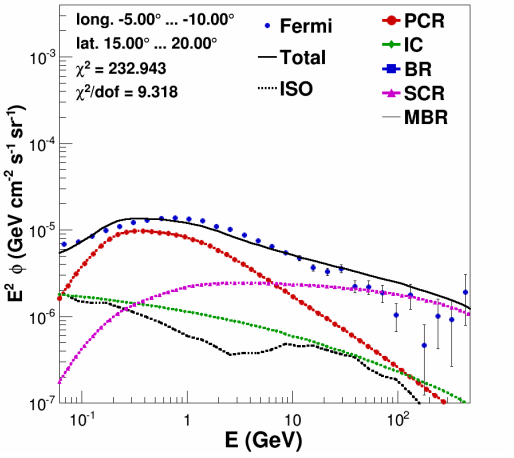


(b) Spectrum from a bubble with background models only and background only.

would expect the MCR emission to be present, if not dominant compared to PCR. Indeed the fit chooses this configuration, with the MCR template dominating all the others and we can directly see the improvement in the MCR fit. The energies around 2GeV had a clear excess that the four components of the SCR fit could not account for. The MCR template peaking in this region, it comes in very handy and fill this gap, Leaving the SCR template taking care of the high energies and PCR and BR for the low energies. **(Why isn't there IC? -> Wait to see if we change the models)** ToDo

### 3.3.1. Discussion on spatial shapes

Fig. **??** shows the spatial distribution of the flux of each component around 2GeV, as returned by the fit.

The bremmstrahlung component is consistent with the the expectations. Present everywhere, it is strong in the disk, and decrease a little in the bubbles.

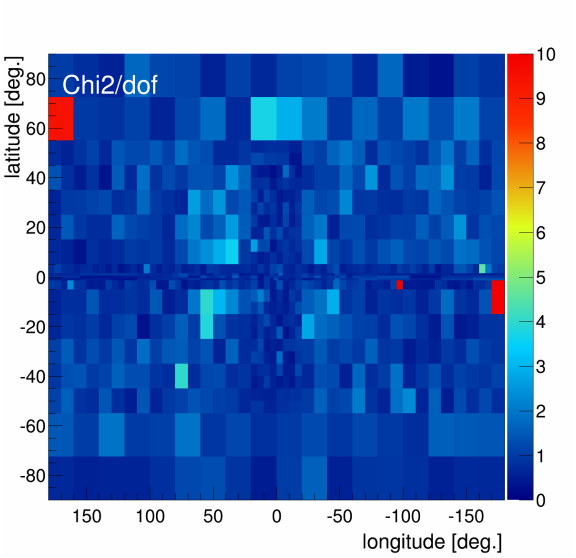


Figure 3.6.: Chi2 maps of MCRonly fits compared to background only

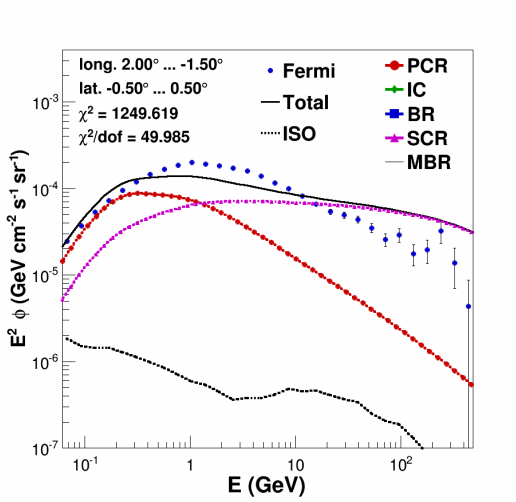


(a) SCR fit in the CMZ region

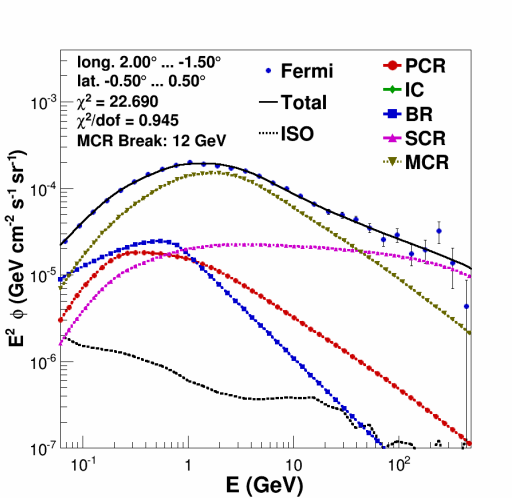


(b) MCR fit in the CMZ region

Though the general shape is sperical, the IC component has an unexpected feature in the form of a strong depletion in the disk, like a "sandwich" structure. This is surprising in the sense that this is where the interstellar radiation field (ISRF) and electron density are supposed to be maximal, creating a higher IC flux. A possible explanation could be coming from the dust distribution, screening the starlight component of the ISRF. Thus depriving the ISRF of its main component and leaving only the dust infra red emission and the CMB to interact with the electrons. This could result in a lower IC gamma-ray flux in the disk.

The SCR component is playing his role perfectly, filling the bubbles and the disk, where the high energy portion of the spectra needs a harder spectrum. It traces perfectly the sources distribution in the disk and the outflow of high energy protons in the bubbles.

The general shape of PCR looks coherent with he shape of the galaxy, with a strong flux in the bar and the galactic disk in general. When looking closely, one can see the same kind of depletion in the disk than for IC, even if the effect is less remarkable. This finds its cause in the MCR distribution with a very high flux in the disk. The sum of both

templates (MCR + PCR) shows no sign of such a feature, which tends to show that some of the PCR photons are absorbed by the MCR template. But the total is coherent, with no unexplainable central gap.

The MCR template also follows the spatial distribution of molecular clouds in our galaxy. It is a good sign since it is supposed to come from those regions. It is not spherical at all. That could have happened if the excess component has a DM origin, since it is supposed to be spherically distributed.

## 3.4. Introducing SCR and DM

The first step is to determine which mass for the WIMP particles would produce the best spectrum for our fit. Fig. 3.9 shows the best fit for the CMZ region, with the WIMP mass as a free parameter. It chooses a mass of 52.3 GeV, peaking around a few GeV, as expected in **(ref theory section)**. Since the excess is the most significant in this region, it is also the best place to define our mass for the rest of the sky. This is what is done in the following section. **ToDo**

Once the mass is determined for the entire sky, the fit gives the following results. The $\chi^2$ distribution (Fig. 3.10 is comparable to the MCR fit for the major part but is significantly worst in the disk.

As seen on Fig. 3.11, the DM distribution of the fit traces closely the distribution of molecular gas distribution (as traced by CO).

## 3.5. Introducing SCR and MSP

The first thing that can be noticed when seeing the $\chi^2$ distribution of the MSP only fit (Fig 3.12) is the similitudes with the DM only fit (Fig. 3.10). The fit succeeds pretty well outside the disk, but gets significantly worst when $|b| < 2$.

Using the MSP spectrum predicted by fermi **(cite)** to fit the CMZ region does not give entire satisfaction. The CMZ is in the disk, where the $\chi^2$ is generally worst. **ToDo**

The distribution of MSP in the sky ressembles the distribution of MCR and DM obtained in previous sections. Present everywhere in the disk, with a higher flux in GC and the bubbles.

**(add picture of residuals at low energy maybe?)** **ToDo**

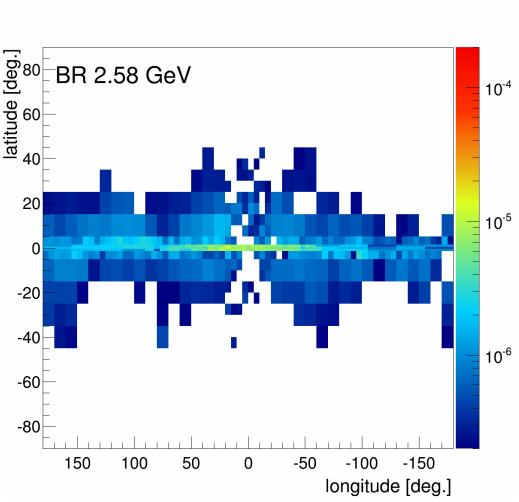


(a) Flux distribution of bremstrahlung (BR)

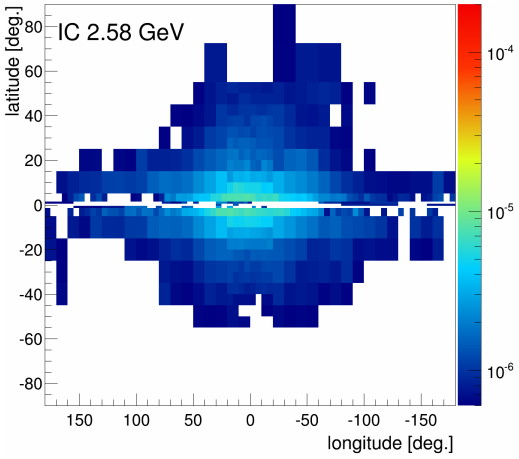


(b) Flux distribution of inverse compton (IC)

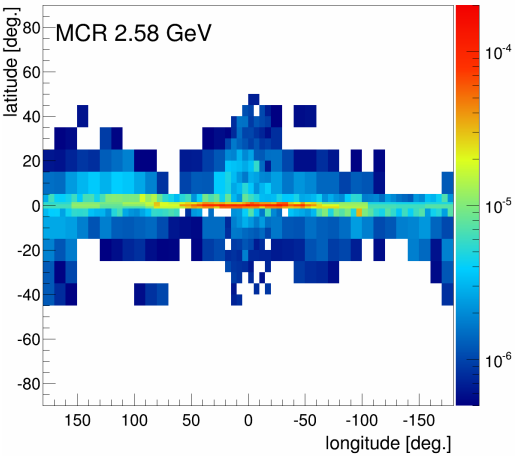


(c) Flux distribution of MCR

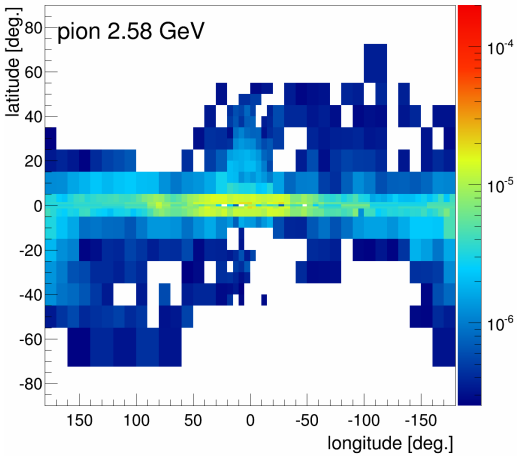


(d) Flux distribution of PCR

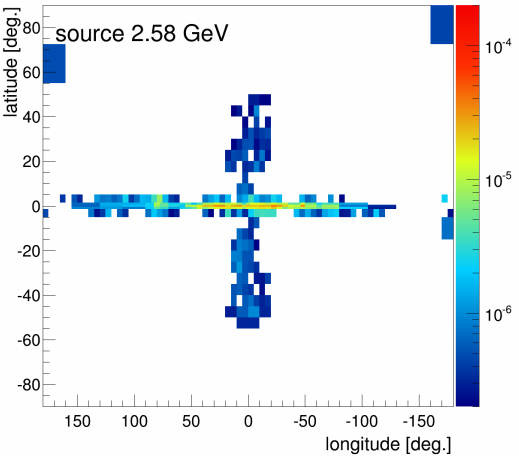


(e) Flux distribution of SCR

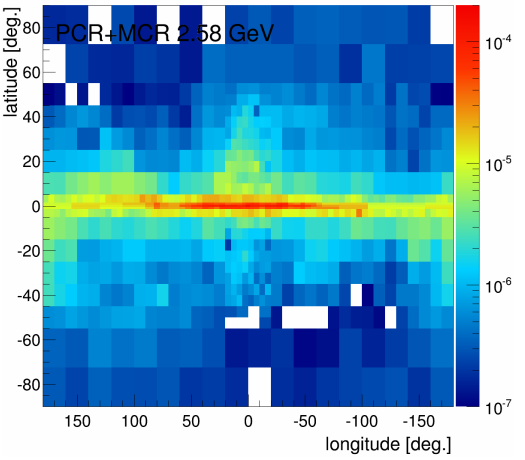


(f) Flux distribution of PCR + MCR

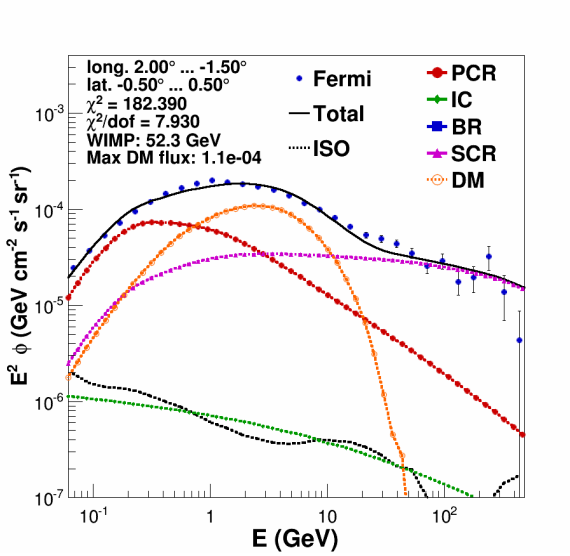


Figure 3.9.: spectrum of best mass DM fitted in CMZ. Also pictures of DM distribution compared to gas map.

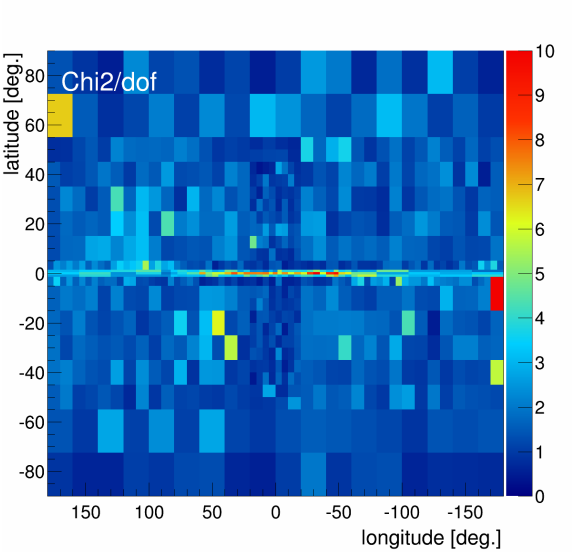


Figure 3.10.: DM fit chi2 distribution

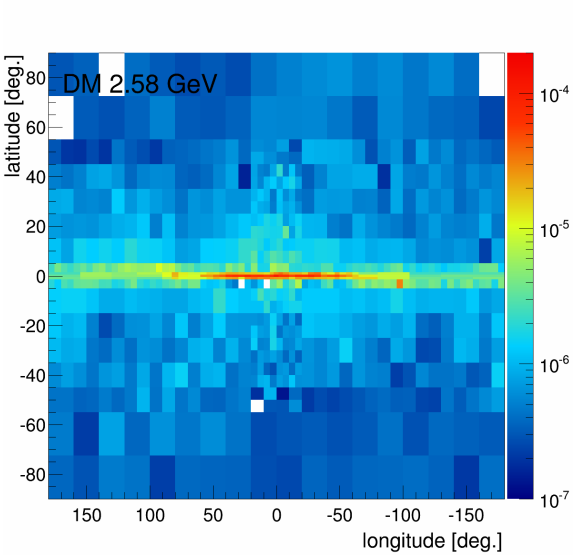


Figure 3.11.: DM distribution compared to gas map.

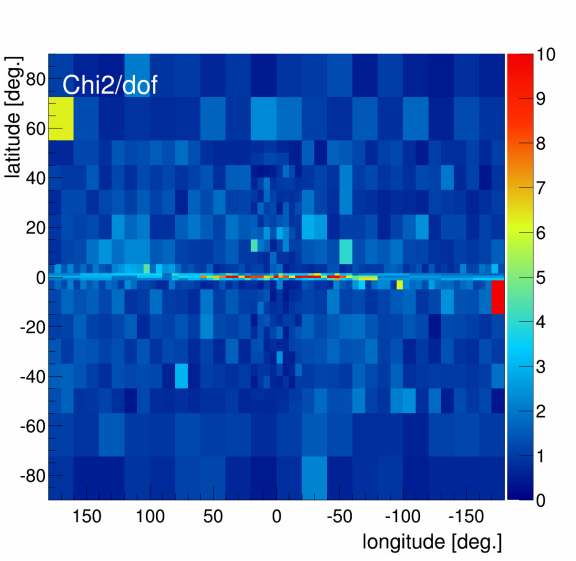


Figure 3.12.: Chi2 distribution of MSP only fit

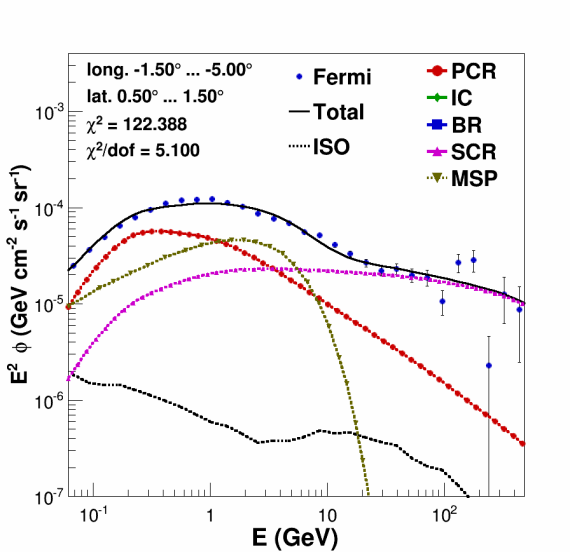


Figure 3.13.: Fit with SCR and MSP spectrum in the CMZ region.

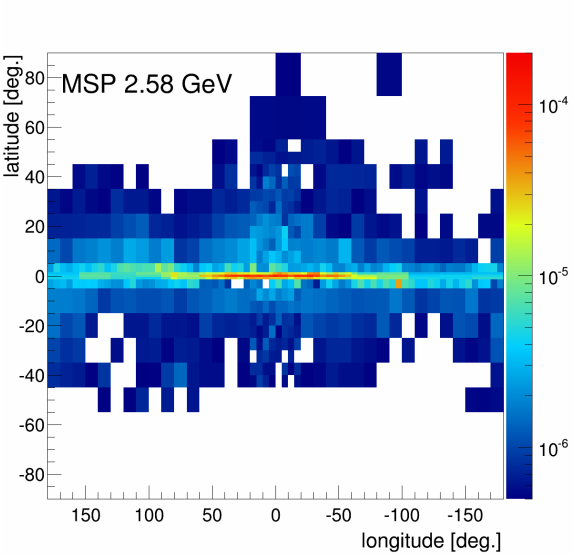


Figure 3.14.: Flux distribution of MSP around 2.5GeV.

# 4. Discussion

## 4.1. Interpretation of spatial shapes

## 4.2. Why is MCR better than DM or MSP

Gavering the results of the previous section, a conclusion tends to emerge : the fit clearly prefers the MCR hypothesis over DM and MSP. We will discuss why in this section.

First of all, comparing the $\chi^2$ skymaps is pretty clear. Adding a fifth component over SCR is a improvement in all cases, but the best fits arre obtained with MCR, especially in the disk.

## 4.3. How do these results fit in context

# 5. Conclusion

Here you write some Conclusion.

# Bibliography

[1] Aguilar, M. et al., *Phys. Rev. Lett.* **2013**, *110*, 141102.

[2] Vagelli, V. Measurement of the cosmic $e^+$+$e^-$ Flux from 0.5 GeV to 1 TeV with the Alpha Magnetic Spectrometer (AMS-02) on the International Space Station. Ph.D. thesis, Karlsruher Institut für Technologie (KIT), 2014.

[3] BibTeX on Wikipedia, `https://en.wikipedia.org/wiki/BibTeX`, Version Date: 2017-09-19.

# List of Figures


1.1. chi2 distribution of first fits (not mines) . . . . . 5
1.2. shape of the excess . . . . . 6

2.1. Figures of data before and after point source subtraction. (Maybe also some spectrum with pass7 and pass8 to see the differences.) . . . . . 7
2.2. Images of the exposure map . . . . . 8
2.3. Systematic error for Pass 8 data. . . . . 10
2.5. . . . . 11
2.6. images of MCR, MSP, DM on single plot. . . . . 12
2.7. Images to illustrate isotropic calibration . . . . . 13

3.1. Some weniger plots to show the GC excess . . . . . 17
3.2. Picture of GC excess, (compare with previous papers?), a chi2 map too . 18
3.3. Picture background only spectra with bad fit (high energies too hard) Compare bubble or disk region and outside . . . . . 18
3.4. Chi2 distribution of SCR only fits. . . . . 19
3.6. Chi2 maps of MCRonly fits compared to background only . . . . . 20
3.9. spectrum of best mass DM fitted in CMZ. Also pictures of DM distribution compared to gas map. . . . . 23
3.10. DM fit chi2 distribution . . . . . 23
3.11. DM distribution compared to gas map. . . . . 24
3.12. Chi2 distribution of MSP only fit . . . . . 24
3.13. Fit with SCR and MSP spectrum in the CMZ region. . . . . 25
3.14. Flux distribution of MSP around 2.5GeV. . . . . 25

# Appendix

## A. Some appendix section

This appendix chapter contains ...